David B. Nash*
Jet Propulsion Laboratory
California Institute of Technology
Pasadena, CA 91103

Detection of Bedrock Topography Beneath a Thin Cover of Alluvium Using Thermal Remote Sensing

Thermal modeling of the annual heating cycle within a granitic bedrock substrate veneered with a thin cover of alluvium indicates that, under desert climatic conditions, thermal remote sensing may detect some topographic features on the bedrock surface through the obscuring cover of alluvium.

Introduction

The feasibility of using thermal remote sensing for indirectly observing topographic relief on a granitic bedrock surface beneath a thin (less than 2 m thick) veneer of loose alluvium in desert regions is examined. This remote sensing technique would provide a means for locating abandoned channels or faults on the surface of buried pediment surfaces (sometimes termed *sub-alluvial benches*) which could be of use in the study of groundwater circulation and for delineating seismically active areas where there may be little or no surface manifestation of faulting (as in the Basin and Range province where alluvium masks or completely buries many pediment surfaces broken by range-front faulting).

The depth to an underlying granitic substrate beneath a thin veneer of alluvium will have a measurable effect on the surface temperature. This depth changes over topographic features on the bedrock and may result in the development of a detectable surface temperature contrast across the feature. By way of introduction to this thermal detection technique, the case of simple cyclical heating is considered (the diurnal and annual heating of the ground surface are both crudely cyclical). If surface temperature T_0, over a given heating cycle of period, P, is assumed a simple harmonic function of time, t, then

$$T_0 = \overline{T}_0 + A_0 \sin(2t\pi/P + \phi) \qquad (1)$$

Abstract: *Modeling of the annual heat flow within a thin alluvium veneer on a granitic bedrock substrate in desert environments, such as found in the southwestern United States, predicts that at certain times of the year the depth to bedrock has a measurable effect on the surface temperature if the alluvium cover is less than 2 m thick. Changes in the thickness of the alluvial cover caused by bedrock topography will produce contrasts in the surface temperature. If temperature contrasts as small as 0.1° C can be resolved, a linear topographic feature having several metres of relief buried by 1.5 m of alluvium may be visible in thermal imagery acquired during January or August in the southwestern U.S. under optimal conditions. Thermal remote sensing may provide a means for delineating some buried faults, fluvial channels, and other features of interest on buried, granitic pediment surfaces.*

where $\overline{T}_0$ is the mean surface temperature during the cycle and ϕ is its phase. The amplitude of the resulting surface temperature cycle, A_0, will be inversely proportional to the thermal inertia, I, of the surface material ($I = \sqrt{KC}$ where K is conductivity and C the volumetric heat capacity). When a high inertia material such as granitic bedrock ($I \approx 5.6 \times 10^{-2}$ cal cm^{-2} s$^{-1/2}$ °K^{-1}) is overlain by a low inertia material such as gravel alluvium ($I \approx 2.5 \times 10^{-2}$ cal cm^{-2} s$^{-1/2}$ °K^{-1}) (Kahle, 1980), the resulting value of A_0 is a progressive, non-linear function of the thickness of the veneering low inertia material

* NASA-National Research Council Resident Research Associate at the Jet Propulsion Laboratory, 1981-1984 (on leave from the Department of Geology, University of Cincinnati, Cincinnati, OH 45221).

Photogrammetric Engineering and Remote Sensing,
Vol. 51, No. 1, January 1985, pp. 77-88.

0099-1112/85/5101-0077$02.25/0

(Van Wijk and Derksen, 1963). With a thin veneer (a few cm) of alluvium, A_0 is strongly influenced by the granite if P is one day or longer. With increasing depth of burial, the granite exerts less influence until, at some threshold of burial, it has no measurable effect on the surface temperature of the overlying alluvium, and A_0 for the alluvium veneered granite is identical to that of alluvium alone. The amplitude (A_z) of the subsurface temperature cycle at a depth z decreases rapidly with depth such that

$$A_z = A_0 \exp(-z/D) \qquad (2)$$

where D is the *thermal skin depth* or *damping depth* ($D = \sqrt{PK/(\pi C)}$) (Van Wijk and De Vries, 1963). At a depth of several skin depths, A_z is negligible and the temperature remains at $\bar{T}_0$. Features located below this depth will have little or no effect on the overlying surface temperature. Because P is 365 times larger for the annual than the diurnal cycle, buried features will be detectable at $\sqrt{365}$ or 19.1 times greater depths when considered over the annual rather than diurnal cycle if the amplitude of the heating cycle and the thermal properties of the materials are kept constant. Although reference will be made to the "diurnal and annual ground temperature *cycle*," the treatment above is too simplified; thus, harmonic heating is not assumed in the model used in this study.

Climatic conditions identical to those in Las Vegas, Nevada during 1978 are used with a realistic, finite differences model of heat flow (modified from Kahle, 1977) to investigate the magnitude of the surface temperature contrast that develops across an alluvium buried depression in granitic bedrock (Figure 1) and the influence depth of burial and season have on this contrast.

Previous Works

The influence that masked or buried objects and materials have on the thermal regime within the overlying, obscuring material has been investigated by geologists, ground water hydrologists, agronomists, and planetologists. Heat flow within an alluvium cover over granitic bedrock is similar, in several respects, to several other systems such as dry soil over a shallow aquifer, or lichens on rocks, or tilled soil over untilled soil. Heat flow in all of these analogous systems and others has been investigated by model and field studies.

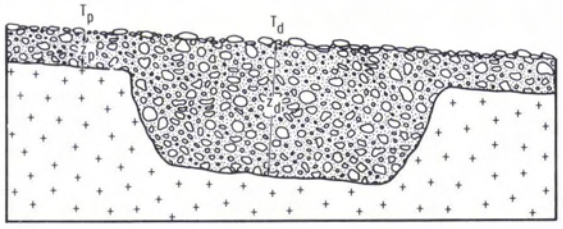

Fig. 1. Cross section through a linear depression on the surface of a granitic pediment buried by a thin (i.e., $z_p <$ 1.5 m) cover of alluvium. A contrast will develop between the surface temperature over the depression, T_d, and the surrounding pediment surface, T_p, that may be detectable in thermal imagery.

Van Wijk and Derksen (1963) use a two-layer soil model to examine the effect of tilling (which produces a loose, low inertia surface layer) on the diurnal and annual surface temperature cycle. Watson (1973) uses an analytical approach to model the diurnal heat flow within lichens ($I \approx 4 \times 10^{-3}$ cal cm^{-2} s$^{-1/2}$ °K^{-1}) or dry sand ($I \approx 1.5 \times 10^{-2}$ cal cm^{-2} s$^{-1/2}$ °K^{-1}) over rock. He finds a 10-cm covering of either lichen or sand is sufficient to mask completely the thermal effects of the underlying rock when considered over a diurnal heating and cooling cycle. Bryne and Davis (1980) report that a 10-cm thick layer of dry peat or dry grass over dry soil (having a higher thermal inertia) yields surface temperatures during the diurnal heating cycle similar to an infinite thickness of the overlying material alone. They further find that, when the thickness of the overlying low thermal inertia layer is less than 10 cm, there is a positive phase shift of the surface temperature cycle of the layered system relative to the surface temperature cycle that would develop on the high inertia material alone. On the basis of his thermal modeling, Pratt (1980) reports a 6-cm thickness of dry sand is sufficient to obscure completely the presence of an underlying layer when considered over the diurnal temperature cycle.

Modeling or field studies of the thermal regime above an aquifer are reported by Cartwright (1968), Birman (1969), Moore and Myers (1972), Myers and Moore (1972), Rosema (1976), Huntley (1978), Tunheim *et al.* (1981), and Heilman and Moore (1981a and 1981b). Saturated soil has an inertia close to that of many rocks ($I \approx 4 \times 10^{-2}$ cal cm^2 s$^{-1/2}$ °K^{-1}), and buried, shallow aquifers have been modeled as simply a high thermal inertia layer beneath a low inertia layer (e.g., Tunheim *et al.*, 1981). Myers and Moore (1972) report detecting the presence of a water table at a depth of from 1.5 to 4.5 m using thermal infrared imagery of a flood plain in South Dakota. On the basis of theory and observation, they suggest that the optimal time for detecting shallow ground water is late August or early September when the temperature contrast between the surface and the ground water is the greatest. However, Huntley (1978) questions what is actually causing the reported thermal anomalies above shallow aquifers and suggests that such anomalies probably are due to higher surface moisture contents and thus larger latent heat fluxes above the aquifer resulting from capillary action.

Thermal Model

A one-dimensional heat flow model is used with an extensive meteorological data base to contrast the surface temperature above a wide but sharp linear

depression on the surface of an alluvium-masked, granitic pediment surface, T_d, with the surface temperature above the surrounding pediment, T_p (Figure 1). The pediment and the bottom of the depression are located at depths of z_p and z_d, respectively, beneath the overlying alluvium. Cooke and Warren (1973) provide a comprehensive discussion of the morphology, distribution, and origin of pediments. Linear depressions may be formed in the otherwise remarkably flat surfaces of pediments by faulting, differential weathering and erosion along joints, faults, and dikes, or by fluvial channel incision.

The model uses a finite differences approach in preference to an analytical approach. Although the finite differences technique is considerably more cumbersome, it readily enables the use of non-cyclical, rapidly varying heat fluxes. Few, if any, of the annual heat fluxes in the following discussion can be adequately described as a single, simple periodic function of time (as assumed in Equation 1).

To model the soil temperature regime, the thermal diffusion equation must be solved with complex, constantly changing, upper boundary conditions. The upper boundary—the ground surface—is heated or cooled by the insolation flux, H_s; the latent heat flux, H_l, resulting from evaporation or condensation of water; the flux conducted into or out of the ground, H_g; the flux absorbed from long wave radiation from the atmosphere, H_d; the flux from long wave radiation from the surface, H_u; and the sensible heat flux between the air and the ground, H_a. Any modeling of the ground surface temperature must satisfy the conversation of energy or

$$H_s + H_l + H_g + H_d + H_u + H_a = 0. \quad (3)$$

Fluxes are considered positive when directed towards the ground surface (directed upward from below the surface or downward from above the surface).

With the exception of H_d, all of the fluxes are simulated with empirical expressions described by Kahle (1977). Only a very brief treatment of these expressions is given here.

LATENT HEAT FLUX, H_l

The latent heat flux is difficult to assess. Although several models use empirical expressions for H_l, including those described by Rosema (1975, 1976), Kahle (1977), Njoku *et al.* (1980), and Kahle *et al.* (1981), as in many other published thermal models, including Watson (1973), Pratt (1980), and Tunheim *et al.* (1981), it is assumed to be negligible in this study. H_l can be quite significant, as indicated in several studies including Sasamori (1970), Rosema (1976), and Kahle *et al.* (1981). Thus, the results of the model study are *only* valid for extreme desert regions where the latent heat flux is quite low. The impact of the latent heat flux on the detectability of buried faults is discussed in a subsequent section of this report.

INSOLATION HEAT FLUX, H_s

The heat flux resulting from solar insolation is simulated with an equation discussed by Kahle (1977) (her Equation 3). The zenith and azimuth angles of the sun are continuously changed over the diurnal and annual cycle. No provision is made for simulating cloud cover or other changes in the short wave transmissivity of the atmosphere, which again limits the applicability of the model to desert regions such as those of the southwestern U.S., which are relatively unclouded. The significance of cloud cover in affecting the detectability of buried faults is assessed later. Although the model can simulate insolation on an inclined surface, a horizontal surface was assumed in this study.

DOWNWARD LONG-WAVE, ATMOSPHERIC, RADIATIVE HEAT FLUX, H_d

Idso and Jackson (1969) propose an empirical equation relating air temperature, T_a, (in °K) at screen height to atmospheric radiation (assumed here to be entirely absorbed).

$$H_d = \sigma T_a^4 \{1 - 0.261 \exp [-7.77 \times 10^{-4} (273 - T_a)^2]\} \quad (4)$$

where σ is the Stefan-Boltzman constant.

UPWARD LONG-WAVE RADIATIVE HEAT FLUX FROM THE GROUND SURFACE, H_u

It will be assumed that the ground surface is a perfect emitter of long-wave radiation; therefore,

$$H_u = -\sigma T_g^4 \quad (5)$$

where T_g is the surface temperature (in °K). Although the ground surface does not actually have an emittance of 1, it is quite high (generally greater than 0.9 for non-vegetated surfaces). As Watson (1981) notes, T_g will decrease while H_u increases with increasing emissivity, and, because these two effects work against each other, the net effect of emissivity variation is reduced.

SENSIBLE HEAT FLUX, H_s

The sensible heat flux is calculated from a simple empirical relationship between the air and ground temperatures (T_a, and T_g, respectively) and wind speed, W, presented by Kahle (1977); i.e.,

$$H_s = C_a C_d W (T_a - T_g) \quad (6)$$

where C_a is the volumetric specific heat of air and C_d is a site specific drag coefficient. A constant of 2 m/s is added to the observed wind speed to account for gustiness. This method for calculating H_s, termed the "bulk aerodynamic" method by Kahle *et al.* (1981), is not as accurate as calculations employing the vertical profile of wind velocity and air

temperature. Schieldge (1978) and Watson (1980) propose techniques for modifying the profile method to use only one measurement of wind velocity and air temperature at a single height. However, Kahle *et al.* (1981) compare values of H_s using the bulk aerodynamic method with values using the profile method and find the overall correlation is good.

FLUX INTO AND OUT OF THE GROUND, H_g

The flux of heat conducted towards or away from the ground surface is proportional to the soil temperature gradient at the surface,

$$H_g = K \frac{\partial T}{\partial z}_{z=0} \tag{7}$$

where z is depth measured down from the ground surface.

HEAT FLOW WITHIN THE GROUND

The flow of heat into and out of the ground will cause a constant change in temperature at a given point in the subsurface temperature profile. The temporal change in temperature is a function of the divergence of the heat flux, or

$$\frac{\partial T}{\partial t} = \frac{\partial}{\partial z}\left(k \frac{\partial T}{\partial z}\right) \tag{8}$$

where k is thermal diffusivity ($k = K/C$). Because k is assumed constant within the alluvium and within the granite, Equation 8 becomes

$$\frac{\partial T}{\partial t} = k \frac{\partial^2 T}{\partial z^2} \tag{9}$$

within each stratum.

In the finite difference solution to Equations 8 and 9, the subsurface temperature profile is represented with an array of points a fixed vertical distance, Δz, apart. Time is incremented in equal steps of Δt duration. $T_{i,j}$ is the temperature at the i^{th} profile and j^{th} time increment. Solution of Equation 9 yields

$$T_{i,j+1} = T_{i,j} + \frac{k\Delta t}{\Delta z^2}(T_{i+1,j} - 2T_{i,j} + T_{i-1,j}). \tag{10}$$

In order to reduce computation time, Δz is allowed to "float" to its maximum stable value for a given value of Δt; i.e.,

$$\Delta z = \sqrt{2k\Delta t} \tag{11}$$

(Δz will thus be different for the alluvium and the granite). Substituting Equation 11 and 10 yields

$$T_{i,j+1} = T_{i,j} + \tfrac{1}{2}(T_{i+1,j} - 2T_{i,j} + T_{i-1,j}). \tag{12}$$

If the boundary between the alluvium and granite occurs at a single profile point, b, Equation 8 becomes

$$T_{b,j+1} = T_{b,j} + \frac{\sqrt{k_g}(T_{b+1,j} - T_{b,j}) - \sqrt{k_a}(T_{b,j} - T_{b-1,j})}{\sqrt{k_g} + \sqrt{k_a}} \tag{13}$$

where k_g and k_a are the thermal diffusivities for the granite and alluvium stratum, respectively. It should be noted that Equation 13 is *only* appropriate if Δz is calculated according to Equation 11 for *each* stratum.

The lower boundary of the temperature profile is assumed to be closed (reflective). Thus, if the profile consists of N profile points, to calculate $T_{N,j+1}$ using Equation 12,

$$T_{N+1,j} = T_{N-1,j}. \tag{14}$$

A geothermal heat flux, H_q, at the lower end of the ground temperature profile may be modeled by

$$T_{N+1,j} = T_{N,j} + \frac{H_q \Delta z}{K}. \tag{15}$$

The inclusion in the model of a geothermal heat flux typical of the southwestern U.S. ($H_q \approx 1 - 2 \times 10^{-6}$ cal s^{-1} cm^{-2}) is found to have little effect on the predicted surface temperature contrast.

Results of the Thermal Model

Values used for the thermal properties of alluvium and granite are listed in Table 1. Hourly wind speed (Figure 2) and air temperatures (Figure 3), collected

Table 1. Thermal Properties of Alluvium and Granite Used in the Model

Parameter	Alluvium	Granite
Volumetric Heat Capacity Cal cm^{-3} °K^{-1} C	0.432	0.416
Thermal Conductivity Cal cm^{-1} °K^{-1} s^{-1} K	1.4×10^{-3}	7.5×10^{-3}
Thermal Diffusivity cm^2/s $k = K/C$	3.24×10^{-3}	1.80×10^{-2}
Thermal Inertia cal cm^{-2} s$^{-1/2}$ °K^{-1} $I = \sqrt{KC}$	2.46×10^{-2}	5.58×10^{-2}
Diurnal Skin Depth cm $D_d = \sqrt{K(86{,}400)/(C\pi)}$	9.44	22.3
Annual Skin Depth cm $D_a = \sqrt{K(31{,}536{,}000)/(C\pi)}$	180.4	425.4

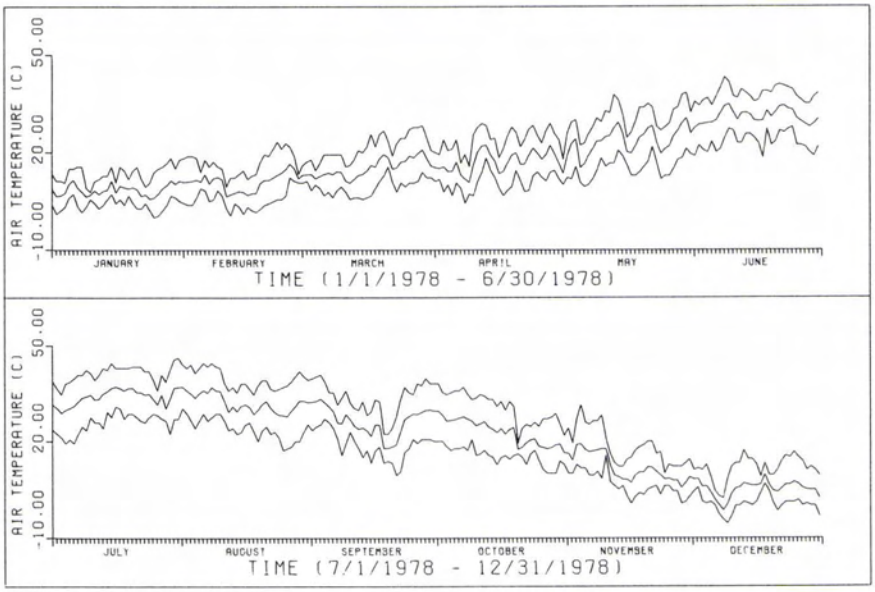

FIG. 2. Daily maximum (upper curve), minimum (lower curve), and mean (middle curve) of hourly air temperature measured at the Las Vegas, Nevada airport during 1978.

by the National Weather Service at Las Vegas, Nevada for 1978, are used to calculate H_d and H_s (Equations 4 and 6, respectively). A value of 1800 s is used for Δt, yielding values of 3.42 cm and 8.06 cm for Δz in the alluvium and granite, respectively. An 18-m temperature profile is considered (the results of the model are very little affected by increasing the profile depth beyond 18 m). It is assumed that the short wave length albedo used in the calculation of H_s is 44 percent (Kahle, 1977).

To investigate the influence of buried granitic bedrock on surface temperature, the hourly surface temperatures calculated by the model are contrasted (differenced) with a "control" case of an 18-m thickness of alluvium alone (Figure 4). The surface temperature of granite veneered with 20 cm of

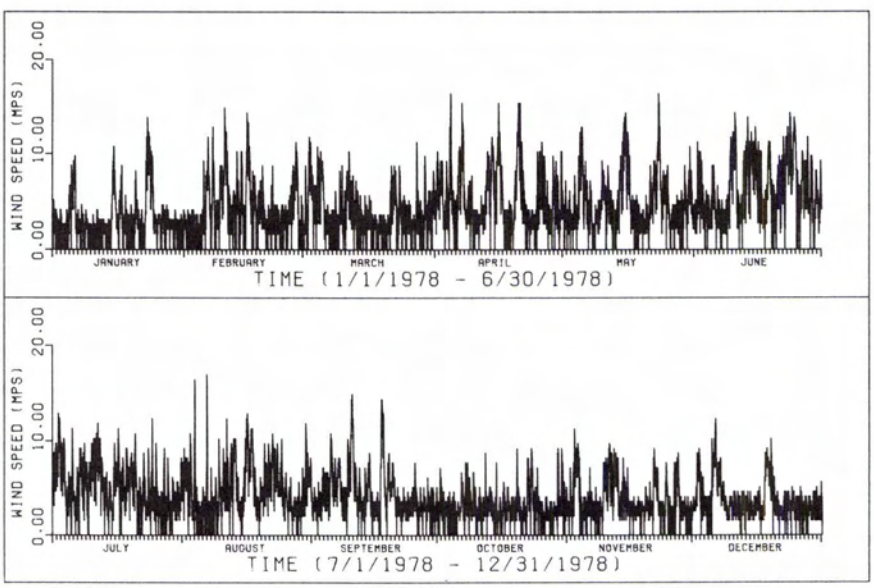

FIG. 3. Hourly wind speed measured at the Las Vegas, Nevada airport during 1978.

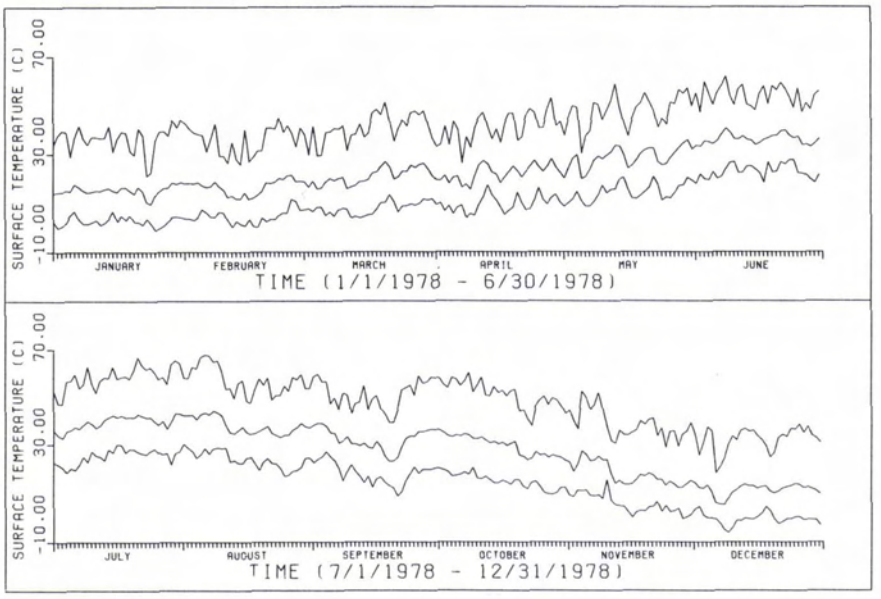

FIG. 4. Daily maximum (upper curve), minimum (lower curve), and mean (middle curve) of hourly ground surface temperature for the alluvium control.

alluvium contrasts strongly with that of the alluvium control (Figure 5). The temperature contrast shows up clearly over the diurnal cycle. The low frequency changes in the contrast result from slow weather changes (Figure 2).

With increasing depth of burial of the bedrock, the temperature contrast decreases rapidly and becomes progressively less obvious over the diurnal heating cycle until it can only be seen over the annual cycle. At a bedrock burial depth of 1 m, broad

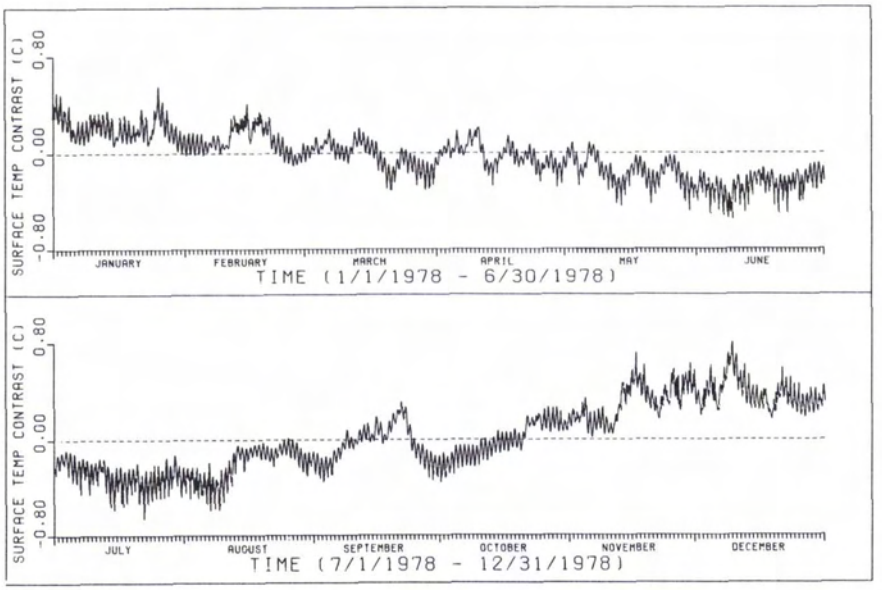

FIG. 5. Hourly surface temperature difference between granite veneered with 20 cm of alluvium and alluvium control (i.e., temperature of veneered granite minus temperature of alluvium alone). The highest frequency changes in contrast occur over the diurnal temperature cycle. The intermediate frequency changes result from wind speed and temperature changes due to passing storms. The lowest frequency contrast change results from the annual temperature cycle.

(i.e., forty day wide) maxima in the surface temperature contrast peak in mid-January and mid-August (Figure 6). During these maxima, high frequency variations in wind speed result in rapid changes in contrast as large 50 percent. The mid-August contrast maximum occurs during a sharp lull in wind speed. These rapid changes in contrast make the optimal time for thermal imagery acquisition difficult to predict.

The maximum values of the temperature contrast predicted for burial depths of the granite from 10 cm to 2 m are shown in Figure 7. With increasing depth of burial, the dates at which the contrast maxima occur are delayed (Table 2). The exact time and date at which a maximum occurs for a given burial depth is determined by high frequency weather changes and will therefore differ slightly from year to year (the time and dates in Table 2 are derived using 1978 weather data from Las Vegas, Nevada).

Although the near surface portion of the temperature profile (depths less than 20 cm) is nearly identical for granite veneered with 1 m of alluvium and for the alluvium control over the diurnal cycle (Figure 8), their temperature profiles at greater depths are substantially different. The presence of buried granite can be detected at deeper depths of burial by using shallow (~2 m) thermistor probes rather than by using surface temperature measurements. Cartwright (1968) and Birman (1969) use such probes to detect the difference in soil temperature above shallow aquifers. The similarities in the temperature profiles of granite veneered with 1 m of alluvium and of the alluvium control are greatest in May and November and least in January and August (Figure 9).

Impact of Simplifying Assumptions

Although it is difficult to determine precisely what impact the simplifying assumptions have on the results of the model, some educated guesses may be made. The detectability of buried granite increases if the contrast between summer and winter ground surface temperatures increases. Most of the simplifying assumptions made in the model will either increase or decrease this contrast, thereby increasing or decreasing the predicted detectability of faulted bedrock.

CLOUD COVER

Cloud cover decreases the amount of insolation energy reaching the surface while decreasing the effective amount of energy radiated from the surface (increases T_{sky}). Geiger (1959) reports the results of a field study of the complex effects of cloudiness on the near surface air temperature. For a summer day, his study finds that, although the amplitude of the diurnal temperature cycle is reduced by several degrees, the average temperature is little affected by cloud cover. However, for a winter day, the average

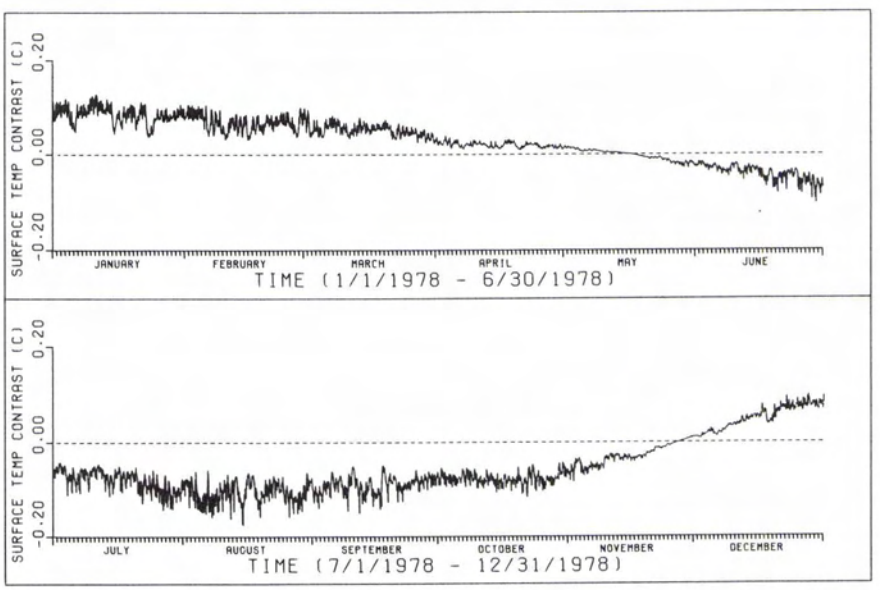

FIG. 6. Hourly surface temperature difference between granite veneered with 1 m of alluvium and alluvium control (temperature of veneered granite minus temperature of alluvium alone). The contrast changes slowly over the annual cycle, producing broad maxima in mid-January and mid-August. The high frequency changes in contrast result from rapid changes in wind speed. The contrast maximum of 15 August corresponds to a sharp lull in wind speed (Figure 3).

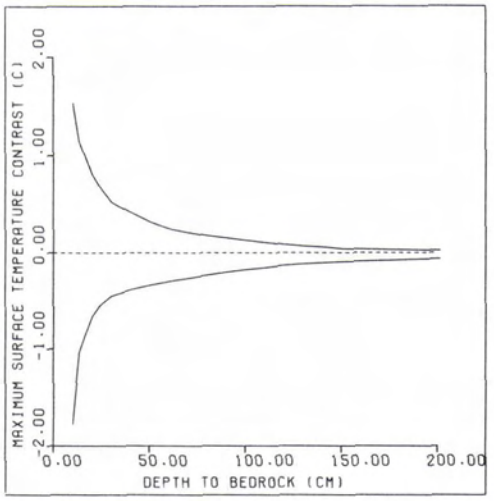

FIG. 7. Maximum yearly positive and negative temperature differences between alluvium veneered granite and alluvium control (temperature of veneered granite minus temperature of alluvium control) as a function of the thickness of the alluvium cover.

temperature is *increased* by several degrees and the amplitude of the diurnal temperature cycle is reduced by cloudiness. If the effect of cloud cover on the surface temperature is similar to the effects on the near surface air temperature, it would reduce the amplitude of the annual ground temperature cycle by increasing the temperature during the winter while leaving the summer temperature unaffected. It is likely that inclusion of the effects of cloudiness into the model would reduce the predicted detectability of faulted bedrock. Thus, the predicted detectability is only valid in relatively cloud free, desert areas.

LATENT HEAT FLUX

Warming and cooling by condensation and evaporation of water will decrease the amplitude of the diurnal ground surface temperature cycle. On the basis of his modeling study, Rosema (1976) finds that the inclusion of the latent heat flux reduces the amplitude of the diurnal surface temperature cycle by as much as 50 percent on a saturated soil with a constant 10 m/s wind velocity. Although he does not examine the impact of the latent heat flux on the amplitude of the annual surface temperature cycle, it is reasonable to assume it is also reduced. It is, thus, likely that the inclusion of the latent heat flux in the model would reduce the detectability of the buried bedrock in a humid climate. However, Vehrencamp (1953) concludes from a field study of a dry playa surface in the Mojave Desert that the latent heat flux is insignificant during the period of observation. Because much of the Basin and Range region is quite arid (less than 10-cm rainfall per year), it is probable that the latent heat flux would not significantly decrease the predicted detectability of buried bedrock.

RAINFALL

Moore and Myers (1972) observe that the specific heat of water is roughly five times that of soil material and that the downward percolation of rainwater will drastically alter the soil temperature profile. It is likely that a significant rainfall would obscure the contrast between T_d and T_p (Figure 1) by establishing nearly identical temperature profiles within the upper surface of the alluvium. A substantial rainfall less than several weeks before the acquisition of the imagery would drastically decrease the detectability of bedrock topography. Rainfall in deserts is generally more frequent in the winter than summer; it is thus more likely that interference from a recent rain storm could be avoided by flying imagery during the summer rather than during the winter temperature contrast maximum.

GROUNDWATER

No provisions are made in the model for the influence of groundwater. The potential effects of groundwater on the detectability of bedrock topography are quite complex. If the groundwater surface is parallel to the ground surface and above the bedrock topography, it would reduce the detectability of the topography, decreasing the contrast between the thermal inertias of the alluvium and the bedrock and, if sufficiently shallow, increasing the evaporative latent heat flux. Moving groundwater could have the effect of maintaining a constant subsurface heat flux, thus also reducing the detectability of bedrock topography. However, if the bedrock topography alters the configuration of the groundwater table or of the groundwater flow (as it frequently does), it is probable that this perturbation would influence the surface temperature and possibly the vegetation pattern.

ANALYSIS AND CONCLUSIONS

This study suggests that, under ideal circumstances, topographic features on granitic bedrock buried by gravel alluvium in hot arid climates may be detected by the surface temperature contrast that develops above the feature. Under such conditions, a thermal imaging system able to resolves temperature differences of $\pm 1°$ C would be sufficient to detect a linear feature with several metres of relief ($z_d - z_p$) veneered with up to 13 cm of alluvium (z_p) (Figure 1). A more sensitive detector able to resolve temperature contrasts of $\pm 0.5°$ C could detect the same feature buried with up to 30 cm of alluvium. A detector with a capacity to resolve temperature differences of $\pm 0.1°$ C would be able to delineate the feature when buried with more than 1 m of alluvium.

TABLE 2. MAGNITUDE, TIME, AND DATE OF MAXIMUM POSITIVE AND NEGATIVE TEMPERATURE CONTRAST BETWEEN GRANITE VENEERED WITH VARIOUS THICKNESSES OF ALLUVIUM AND AN ALLUVIUM CONTROL

Depth to Granite (cm)	Maximum Negative Contrast			Maximum Positive Contrast		
	$T_{\text{Veneered Granite}} - T_{\text{Alluvium Control}}$ (°C)	Time*	Date	$T_{\text{Veneered Granite}} - T_{\text{Alluvium Control}}$ (°C)	Time*	Date
10.25	1.78	19:00	6/8	1.53	7:00	11/25
13.66	1.03	19:00	6/8	1.14	11:00	12/9
20.49	0.66	17:00	7/22	0.80	18:00	12/9
23.91	0.56	5:00	7/22	0.69	18:00	12/9
30.74	0.45	5:00	7/22	0.52	18:00	12/9
40.99	0.38	8:00	8/12	0.41	23:00	12/12
51.23	0.33	8:00	8/12	0.31	23:00	12/12
61.48	0.29	8:00	8/12	0.24	8:00	12/17
68.31	0.27	8:00	8/12	0.22	3:00	1/4
78.56	0.24	8:00	8/12	0.18	7:00	1/11
88.81	0.20	8:00	8/12	0.15	7:00	1/11
99.05	0.18	8:00	8/12	0.13	7:00	1/11
109.30	0.16	8:00	8/12	0.11	7:00	1/11
119.55	0.13	8:00	8/12	0.08	7:00	1/11
129.79	0.11	2:00	9/12	0.07	8:00	3/1
140.04	0.10	2:00	9/12	0.06	8:00	3/1
150.28	0.09	2:00	9/12	0.04	8:00	3/1
201.52	0.06	4:00	10/22	0.02	23:00	4/9

Based on hourly wind speed and air temperature data from Las Vegas, Nevada collected during 1978.
* Local time (PST)

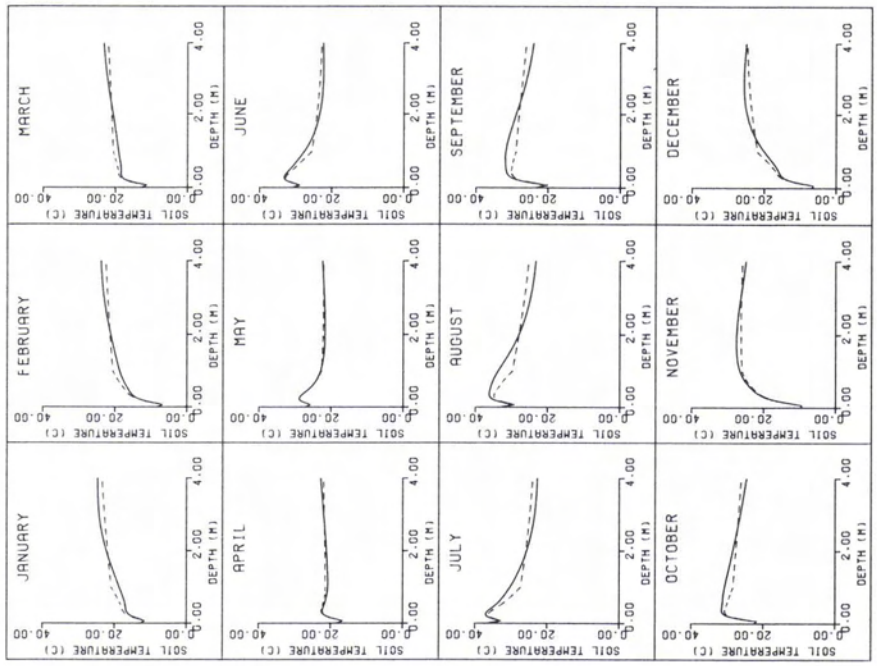

FIG. 9. Upper 4 m of the ground temperature profile for alluvium control (solid line) and granite veneered with 1 m of alluvium (dashed line) over the annual cycle for the fifteenth of each month at 8:00 AM.

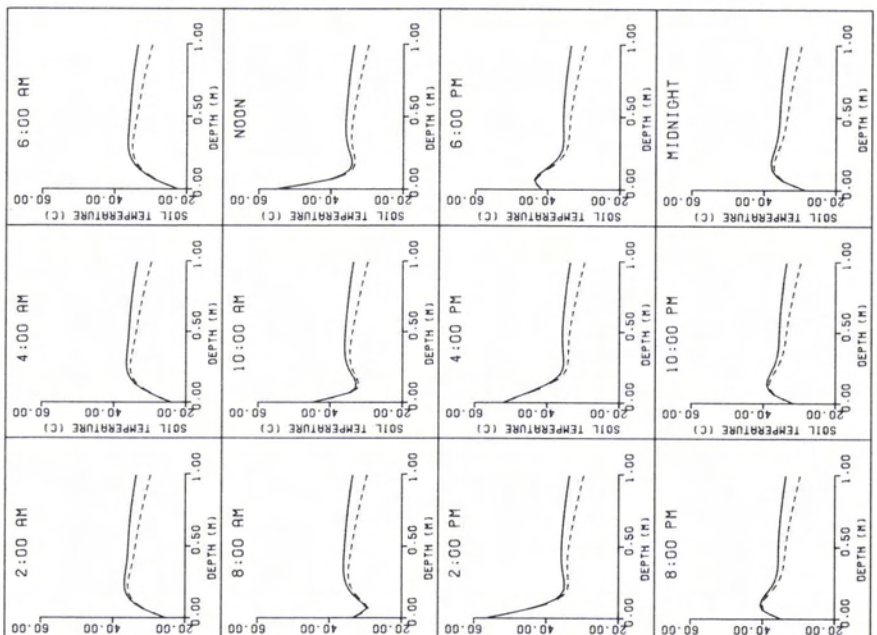

FIG. 8. Upper 1 m of the ground temperature profile for alluvium control (solid line) and granite veneered with 1 m of alluvium (dashed line) over the diurnal cycle for 15 August.

The detectability of bedrock topography increases as the thermal inertia of the bedrock increases. Several rock types have thermal inertias higher than granite including dolomite ($I \approx 7.5 \times 10^{-2}$ s$^{-1/2}$ °K^{-1}) and basic and ultrabasic rock types ($I \approx 5.5 - 8.4 \times 10^{-2}$ cal cm^{-2} s$^{-1/2}$ °K^{-1}) (Kahle, 1980). Buried topography on these bedrock types could be detected at depths greater than detectable for granitic bedrock.

Several factors will either degrade the sharpness of the surface temperature contrast across buried bedrock topography or otherwise decrease its detectability in thermal imagery. Lateral flow of heat in the alluvium will cause the temperature contrast to be reduced and spread over a zone wider than the width of the bedrock feature. Areal inhomogeneities in the alluvium veneer, including differences in the thermal properties and albedos of individual rock clasts and in plant cover such as creosote bushes, introduce "noise" to remotely measured surface temperatures having an amplitude larger than the temperature contrast across the bedrock feature. Much of this noise will be eliminated by using a scanner with an instantaneous field of view (IFOV) larger than the spatial frequency of the areal inhomogeneities. Because the spatial frequency of some of the inhomogeneities is quite large, a scanner with a large IFOV (perhaps 10- to 20-m wide) and a high temperature resolution will be best suited for detecting large linear features such as faults and channels. Creosote bushes will also influence the energy balance at the ground surface by shading it from the sun and sheltering it from the wind. Fortunately, these bushes often are uniformly and sparsely distributed in very arid regions.

Although lateral heat flow and areal inhomogeneities make buried bedrock topography more difficult to detect in thermal imagery, features such as faults, joints, and channels frequently are remarkably linear; thus, the diffuse surface temperature contrast above the feature will also be quite linear. Linear features are relatively easy to find in imagery; enhancement and filtering of digital imagery make them even more detectable.

Latent heat flux and the influence of clouds are not considered in this study, thus limiting the applicability of the results to relatively cloud-free, hot, sparsely vegetated deserts. Despite this limitation, such deserts are fairly extensive throughout the world. Range-front faults in the arid areas of the southwest U.S. should be particularly amenable to detection by the technique described here. The optimal times of year for detecting thermal contrasts over faults in granitic bedrock buried with over 50 cm of alluvium are mid-January and mid-August, but the surface temperature contrast is not significantly reduced during the preceding or following 20 days. High frequency changes in the wind velocity result in rapid and large (50 percent) changes in the surface temperature contrast. Although the model results indicate that the maximum temperature contrasts often occur during the early and late daylight periods, it may be more practical to acquire nighttime imagery when linear features resulting from cloud trials and differences in albedo are at a minimum. The thermal image should be collected in digital form so that it may be subsequently enhanced for detecting linear features.

The predictions made in this study have been tested and confirmed in a field investigation of a faulted pediment surface in the Mojave desert, California. The results of that study will be presented in a forthcoming article. Blom *et al.* (1984) have recently demonstrated the ability of radar to detect shallow subsurface features in another, nearby area in the Mojave desert. A comparison of the relative detecting abilities of thermal and radar remote sensing is planned.

Acknowledgments

This work was done while the author was a NASA-National Research Council resident research associate at the Jet Propulsion Laboratory, California Institute of Technology, under the supervision of Dr. Anne B. Kahle. Dr. Kahle is thanked for her guidance and for sharing her thermal modeling expertise. The author gratefully acknowledges the many suggestions and contributions of Drs. Anne B. Kahle and Frank D. Palluconi. The research described in this paper was carried out by the Jet Propulsion Laboratory, California Institute of Technology, under contract with the National Aeronautics and Space Administration.

References

Birman, J. H. 1969. Geothermal exploration for groundwater. *Geological Society of America Bulletin*, 80:617-630.

Blom, R. G., R. E. Crippen, and C. Elachi, 1984. Detection of subsurface features in SEASAT radar images of Means Valley, Mojave Desert, California. *Geology*, 12:346-349.

Byrne, G. F., and J. R. Davis, 1980. Thermal inertia, thermal admittance and the effect of layers. *Remote Sensing of Environment*, 9:295-300.

Cartwright, K., 1968. *Temperature Prospecting for Shallow Glacial and Alluvial Aquifers in Illinois*. Illinois State Geological Survey Circular 433. Illinois Geological Survey, Urbana. 41p.

Cooke, R. V., and A. Warren, 1973. *Geomorphology in Deserts*. University of California Press, Berkeley, 394p.

Geiger, R., 1959. *The Climate Near the Ground*, trans. by N. M. Stewart and others. Harvard University Press, Cambridge, 494p.

Heilman, J. L., and D. G. Moore, 1981a. Soil moisture applications of Heat Capacity Mapping Mission, in *Evaluation of HCMM Data for Assessing Soil Moisture and Water Table Depth*, Final Report, contract NAS5-24209, NASA pp. 78-95.

———, 1981b. Groundwater application of the Heat Capacity Mapping Mission, in *Evaluation of HCMM*

Data for Assessing Soil Moisture and Water Table Depth, Final Report, Contract NAS5-24209, NASA. pp. 109-119.

Huntley, D., 1978. On the detection of shallow aquifers using thermal infrared imagery. *Water Resources Research*, 6:1075-1083.

Idso, S. B., and R. D. Jackson, 1969. Thermal radiation from the atmosphere. *Journal of Geophysical Research*, 74:5397-5403.

Kahle, A. B., 1977. A simple thermal model of the Earth's surface for geologic mapping by remote sensing. *Journal of Geophysical Research*, 82:1673-1680.

———, 1980. Surface thermal properties, in *Remote Sensing in Geology* (B. S. Siegal and A. R. Gillespie, eds). John Wiley and Sons, New York. pp. 258-273.

Kahle, A. B., J. P. Schieldge, M. J. Abrams, R. F. Alley, and C. J. LeVine, 1981. *Geological Application of Thermal Inertia Imaging Using HCMM Data*, Jet Propulsion Laboratory Publication 81-55, Pasadena. 199p.

Moore, D. G., and V. I. Myers, 1972. *Environmental Factors Affecting Thermal Groundwater Mapping*, Technical Report SDSU-RSI-72-06 for USGS Contract No. 14-08-001. Remote Sensing Institute, Brookings, 23p.

Myers, V. I., and D. G. Moore, 1972. Remote sensing for defining aquifers in glacial drift. *Proceedings of the Eighth International Symposium on Remote Sensing of Environment*, Environmental Research of Michigan, Ann Arbor, pp. 715-728.

Njoku, E. G., J. P. Schieldge, and A. B. Kahle, 1980. *Joint Microwave and Infrared Studies for Soil Moisture Determination*, Jet Propulsion Laboratory Publications 81-55, Pasadena. 199p.

Pratt, D. A., 1980. Two-dimensional model variability in thermal inertia surveys, *Remote Sensing of Environment*, 9:325-338.

Rosema, A., 1975. Simulation of the thermal behavior of bare soils for remote sensing purposes, in *Heat and Mass Transfer in the Biosphere—Part I, Transfer Processes in the Plant Environment* (D. A. de Vries and N. H. Afghan, eds). John Wiley and Sons, New York. pp. 109-123.

———, 1976. Heat capacity mapping, is it feasible? *Proceedings of the Tenth International Symposium on Remote Sensing of Environment*, Environmental Research Institute of Michigan, Ann Arbor, pp. 571-584.

Sasamori, T., 1970. A numerical study of atmospheric and soil boundary layers. *Journal of the Atmospheric Sciences*, 27:1122-1137.

Schieldge, J. P., 1978. On estimating the sensible heat flux over land. *Agricultural Meteorology*, 9:315-328.

Tunheim, J. A., G. A. Beutler, and S. D. Ness, 1981. Model development for monitoring water tables and near surface moisture by thermography, in *Evaluation of HCMM Data for Assessing Soil Moisture and Water Table Depth*, Final Report, Contract NAS5-24209, NASA. pp. 143-199.

Van Wijk, W. R., and W. J. Derksen, 1963. Sinusoidal temperature variation in a layered soil, in *Physics of Plant Environments* (W. R. Van Wijk, ed). John Wiley and Sons, New York, pp. 171-209.

Van Wijk, W. R., and D. A. De Vries, 1963. Periodic temperature variations in a homogeneous soil, in *Physics of Plant Environments* (W. R. Van Wijk, ed). John Wiley and Sons, New York. pp. 109-123.

Vehrencamp, J. E., 1953. Experimental investigation of heat transfer at an air-earth interface, *American Geophysical Union Transaction*, 34:22-30.

Watson, K., 1973. Periodic heating of a layer over a semi-infinite solid. *Journal of Geophysical Research*, 78:5904-5910.

———, 1980. Direct computation of the sensible heat flux. *Geophysical Research Letters*, 7:616-618.

Watson, K., S. Hummer-Miller, and T. W. Offield, 1981. *Geological Application of Thermal-Inertia Mapping from Satellite*, Final Report, HCMM investigation S-40256-B, Goddard Space Flight Center. 72p.

(Received 8 September 1982; revised and accepted 28 August 1984)

Special Invitation

The Engineering Applications Committee of the ASP Remote Sensing Applications Division wish to hold a special session on *Remote Sensing Solutions to Engineering Problems in New Frontier Areas* at the 1986 Fall Technical Meeting in Anchorage, Alaska. The committee welcomes early proposals for papers on this topic.

For further information please contact

Mr. Geoff Tomlins
B.C. Research Council
3650 Westbrook Mall
Vancouver, B.C. V6S 2L2, Canada
Tele. (604) 224-4331